

UNCLASSIFIED

Defense Technical Information Center
Compilation Part Notice

ADP012882

TITLE: Progress in Red Vertical Cavity Surface Emitting Lasers

DISTRIBUTION: Approved for public release, distribution unlimited

Availability: Hard copy only.

This paper is part of the following report:

TITLE: Nanostructures: Physics and Technology. 7th International Symposium. St. Petersburg, Russia, June 14-18, 1999 Proceedings

To order the complete compilation report, use: ADA407055

The component part is provided here to allow users access to individually authored sections of proceedings, annals, symposia, etc. However, the component should be considered within the context of the overall compilation report and not as a stand-alone technical report.

The following component part numbers comprise the compilation report:

ADP012853 thru ADP013001

UNCLASSIFIED

Progress in red vertical cavity surface emitting lasers

J. A. Lott

Air Force Institute of Technology, Wright-Patterson AFB, Ohio USA

Abstract. The development of red vertical cavity surface emitting lasers with peak emission wavelengths from 620 to 690 nm is reviewed. The performance characteristics of state-of-the-art gain guided and selectively oxidized device structures are presented.

1 Introduction

Red (620–700 nm) vertical cavity surface emitting lasers (VCSELs) are candidates for plastic fiber communications, compact disk and digital video disk holographic heads, medical diagnostics, and optical alignment and interconnects. The devices consist of an AlGaInP quantum well optical cavity active region surrounded by AlGaAs distributed Bragg reflectors (DBRs). To avoid absorptive losses, the AlAs mole fraction (x) of the higher index/lower bandgap $\text{Al}_x\text{Ga}_{1-x}\text{As}$ DBR quarter-wave layer is increased as the desired emission wavelength is decreased. As determined from Fig. 1, this requires that $x > 0.4$ for peak emission wavelengths below 700 nm. The value of x should increase to about 0.6 for peak emission at 630 nm.

Optically-pumped “visible” (peak emission at 740 nm) VCSELs were first reported in 1987 [1], followed by AlGaAs VCSEL diodes (770 nm) in 1991 [2] and AlGaInP VCSEL diodes (639–661 nm) in 1993 [3]. Many other reports of visible VCSELs have followed [4–8]. As with near-infrared (800–1000 nm) VCSELs, improved performance has

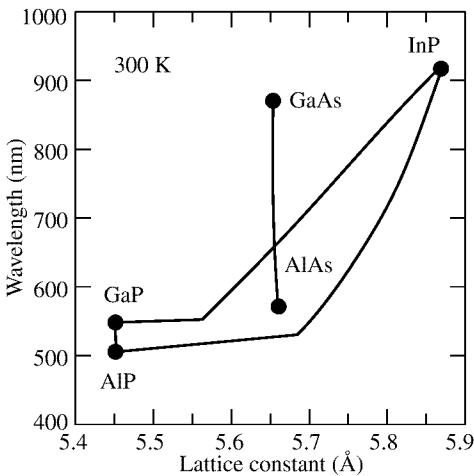


Fig. 1. Photon wavelength vs. lattice constant for AlGaAs and AlGaInP.

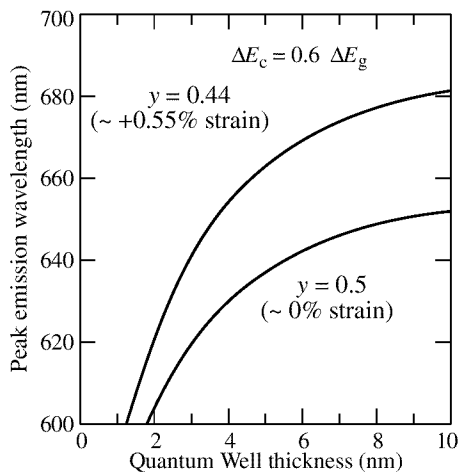


Fig. 2. Calculated room temperature peak emission wavelength vs. QW thickness. The curves are for $\text{Ga}_y\text{In}_{1-y}\text{P}$ ($y = 0.44, 0.5$) QWs with $(\text{Al}_{0.5}\text{Ga}_{0.5})_{0.5}\text{In}_{0.5}\text{P}$ barrier layers.

been obtained by moving from simple pillar structures to gain-guided proton implanted structures, and to new native Al-oxide structures [9]. Other parallel improvements include DBR interface grading and pulse doping schemes. This paper reviews the development and performance characteristics of proton implanted and native Al-oxide red VCSEL structures from 1991 to the present.

2 Device structures

The VCSELs are grown by low pressure metalorganic vapor phase epitaxy on (100) (n^+)GaAs substrates, misoriented 5° or 10° toward the (111)A. The top (n) and bottom (p) DBRs are composed of $Al_xGa_{1-x}As$ ($x = 0.5$ or 0.6)/ $Al_xGa_{1-x}As$ ($x = 0.92$ or 1.0) with graded interfaces. The p-dopant is C, while the n-dopant is Si. The first low index DBR layer on top of the optical cavity is composed of $Al_xGa_{1-x}As$ ($x = 1.0$). The one-lambda optical cavity active region has three or four, 6–8 nm-thick, $Ga_yIn_{1-y}P$ ($y = 0.42-0.5$) QWs surrounded by undoped $(Al_{0.5}Ga_{0.5})_{0.5}In_{0.5}P$ barrier layers. For reference, Fig. 2 shows the calculated peak emission wavelength for example AlGaInP QW active regions as a function of QW thickness.

The optical properties of AlGaInP are influenced by an ordered phase that occurs naturally, under certain crystal growth conditions, on the group III sublattice [10]. Long range ordering is directly related to a reduction in the GaInP energy bandgap (up to ~ 130 meV) as compared to fully disordered (random) epitaxial layers. The effects of ordering are clearly observed in the photoluminescence (PL) spectra of Fig. 3. The PL peaks in curves (b) and (d), as compared to those in curves (a) and (c), are broadened and shifted toward longer wavelengths, indicating increased ordering. In this case, a reduction in ordering is obtained by increasing the misorientation of the substrates from 2° to 5° off (100), and increasing the growth temperature from 675 to 750 °C.

The 2-inch diameter wafers are grown without rotation, resulting in a thickness variation along the centerline from front to back. This is an important research technique for fabricating prototype devices, allowing the characterization of devices with varying mismatch

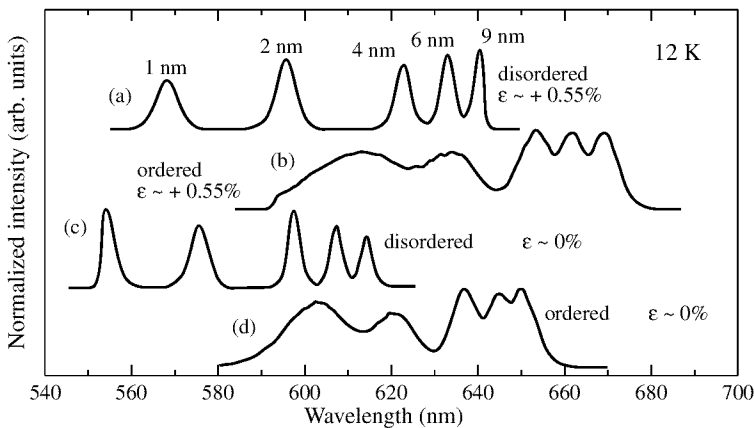


Fig. 3. Photoluminescence of AlGaInP QW heterostructures with five $Ga_yIn_{1-y}P$ QWs that are 9, 6, 4, 2, and 1 nm thick, separated by 60 nm thick $(Al_{0.7}Ga_{0.3})_{0.5}In_{0.5}P$ barrier layers. Curves (a) and (c): $T_g = 750^\circ C$, 6° off (100) substrate. Curves (b) and (d): $T_g = 675^\circ C$, 2° off (100) substrate.

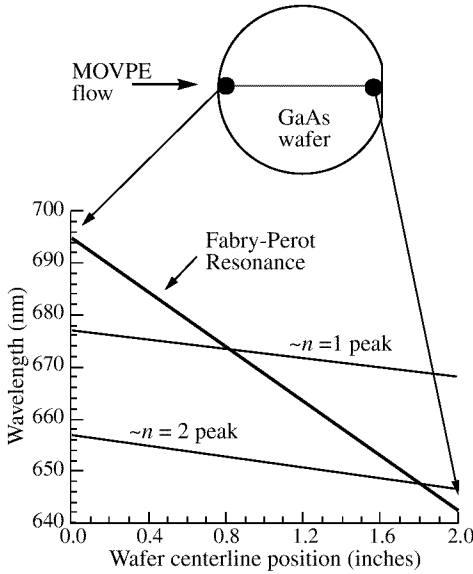


Fig. 4. Schematic of the variation in Fabry–Perot resonance wavelength and peak QW transition wavelengths across an unrotated red VCSEL wafer ($n = 1$ and $n = 2$ refer to the first and second quantized state QW transitions).

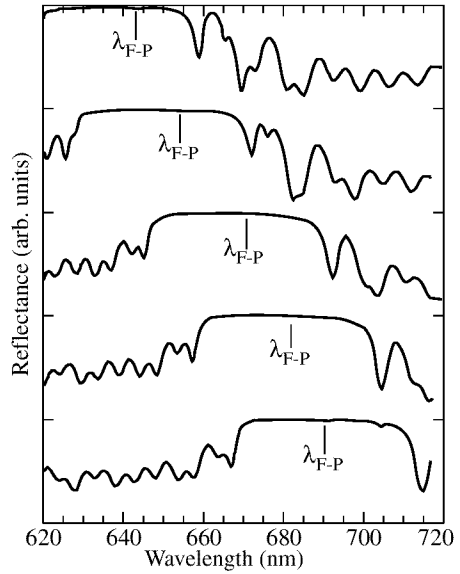


Fig. 5. Measured reflectance spectra (at normal incidence) at five approximately equally spaced points across a nonrotated red VCSEL wafer.

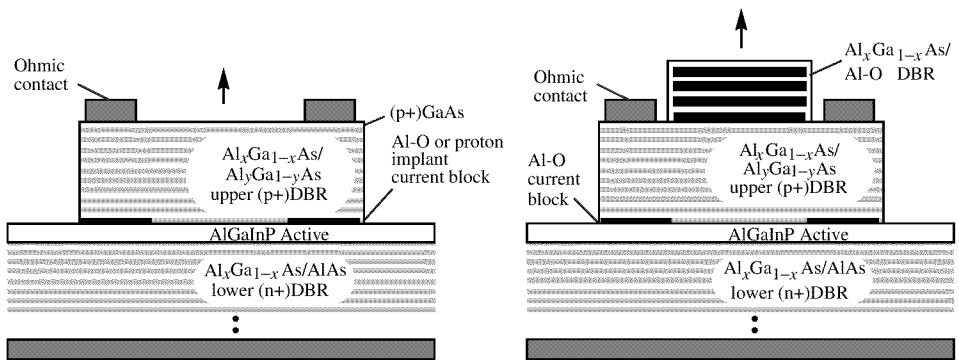


Fig. 6. Schematic diagrams of a proton implanted (gain guided) or Al-oxide red VCSEL (left), and a selectively oxidized red VCSEL with a partial top Al-oxide DBR (right).

between the Fabry–Perot resonance and the QW gain peak. Figure 4 shows the measured variation in Fabry–Perot resonance and peak gain for a typical wafer. The small variation in QW gain results primarily from a change in GaInP QW composition across the nonrotated wafer. The measured reflectance spectra for an example nonrotated red VCSEL wafer is shown in Fig. 5. The wafers are fabricated into ion implanted or selectively oxidized Al–O structures as shown in Fig. 6. The fabrication proceeds in a manner similar to that described in [6–9].

Table 1. Typical CW performance characteristics of proton implanted (H^+) and selectively oxidized (Al-O) VCSELs at 300 K. The emission apertures are approximately $5 \times 5 \mu m^2$. The maximum power conversion efficiency is given by η_{max} . The maximum output power P_{max} is for the fundamental transverse mode.

	690 nm		650 nm		630 nm	
	H^+	Al-O	H^+	Al-O	H^+	Al-O
I_{th} (mA)	1.2	0.5	3.5	0.8	5.2	2.1
V_{th} (V)	2.4	2.0	2.7	2.2	3.1	2.2
P_{max} (mW)	6.5	9	1.0	2	0.1	0.35
η_{max} (%)	18	45	5	35	0.5	12

3 Performance characteristics

Typical continuous wave (CW) performance characteristics for selectively oxidized red VCSELs are shown in Fig. 7 and Fig. 8. As with red edge-emitting lasers, the maximum output power decreases and the threshold current increases as the emission wavelength decreases. A summary comparison between implanted and selectively oxidized VCSELs is given in Table 1 (for structures based on Fig. 6, left). The values are the averages of 20 randomly selected devices emitting within 5% of the given peak wavelength. The gain guided device performance rivals that of conventional gain guided infrared (850, 980 nm) VCSELs circa 1992. The selectively oxidized red VCSEL performance for emission at 690 nm is roughly equal to the best state-of-the-art infrared VCSELs emitting at 850 nm. Life tests were performed on the 690 nm Al-oxide VCSELs at 50 °C. After 2000 hours, the threshold currents and voltages, and peak output powers remain within 3% of their starting values.

4 Resonant mode blueshifts in microcavity VCSELs

Conventional planar VCSELs support a single longitudinal optical mode and one or more transverse optical modes. Intracavity Al-oxide layers are selectively positioned within a VCSEL to form both a current aperture and a cylindrical or rectangular waveguide. A Microcavity VCSEL is formed when the radius of the VCSEL’s transverse aperture is on the

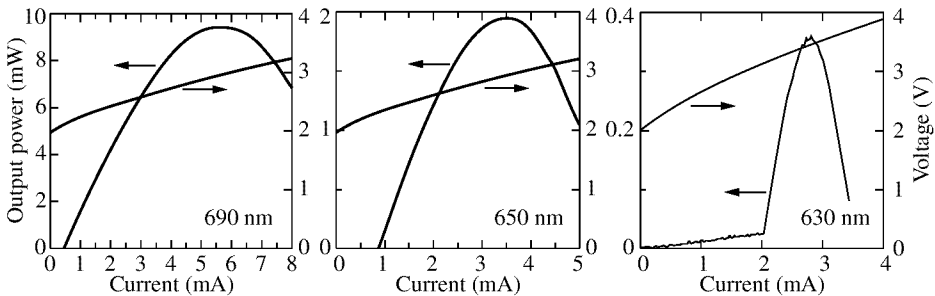


Fig. 7. Room temperature L-I characteristics for selectively oxidized red VCSELs emitting at 690, 650, and 630 nm. The oxide apertures are approximately $5 \times 5 \mu m^2$.

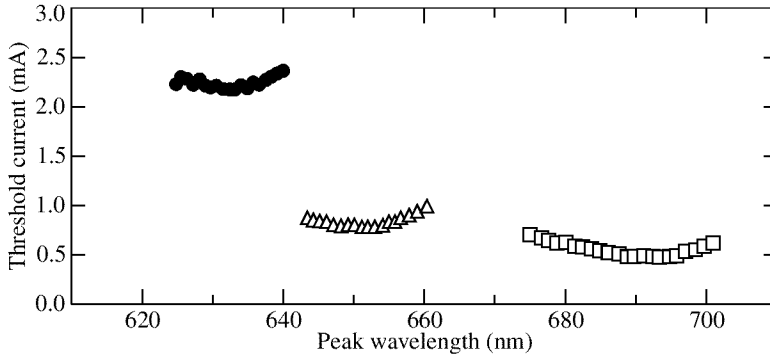


Fig. 8. Room temperature threshold current versus peak emission wavelength for selectively oxidized red VCSELs emitting near 690, 650, and 630 nm. The oxide apertures are approximately $5 \times 5 \mu\text{m}^2$.

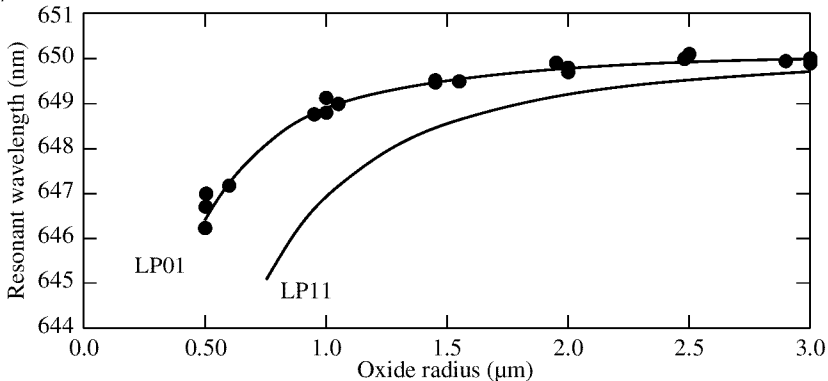


Fig. 9. Calculated (solid lines) and measured (dots) room temperature resonant emission wavelength as a function of oxide aperture radius for selectively oxidized red VCSELs designed for large area emission at 650 nm. The fundamental (LP01) and first higher order mode (LP11) are shown.

order of the thickness of the VCSEL's longitudinal resonant microcavity [11]. The lasing modes for large area VCSELs are one-dimensional quasi-plane waves, whereas the lasing modes of microcavity VCSELs are true three-dimensional modes. From a purely optical point of view, the resonant modal wavelengths of red and near infrared VCSELs blueshift as the aperture radius decreases below about $5 \mu\text{m}$. Consider a circularly symmetric, oxide aperture VCSEL designed for large area emission at 650 nm (Fig. 6, left). Figure 9 is a plot of the calculated [12] (and measured) resonant mode blueshift for this VCSEL as the radius of the oxide aperture is varied from $3 \mu\text{m}$ down to $0.5 \mu\text{m}$. The fundamental and first higher order modes for the 650 nm VCSEL are illustrated in Fig. 10.

5 Conclusion

Red AlGaInP/AlGaAs VCSELs have reached maturity and are ready to be used in a variety of photonic systems. Superior overall performance is obtained for devices with emission wavelengths from 660 to 690 nm. Devices emitting between 630 to 660 nm will eventually become commercially viable. Future optical interconnect and related photonic systems may well be based on dense arrays of red or infrared VCSELs. When implementing these

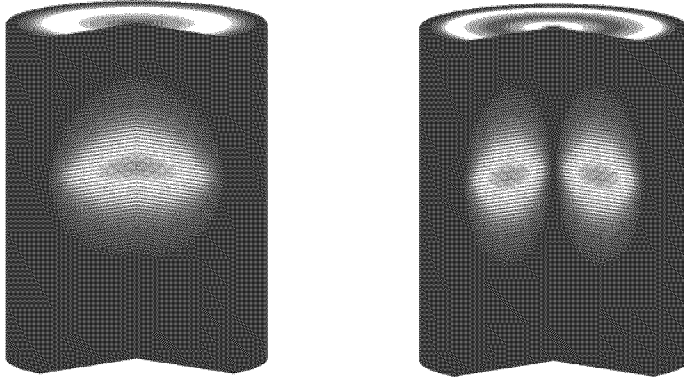


Fig. 10. Calculated fundamental mode (LP01, left) and first higher order mode (LP11, right) optical energy profile for a 650 nm selectively oxidized (single Al–O layer) VCSEL. The energy distribution on the top surface is amplified in order to illustrate the emitted mode.

arrays with small diameter VCSELs, one may need to account for resonant mode blueshifts (along with resonant mode redshifts due to device heating).

References

- [1] P. L. Gourley and T. J. Drummond, *Appl. Phys. Lett.* **50**, 1225 (1987).
- [2] Y. H. Lee, B. Tell, K. F. Brown-Goebeler, R. E. Leibenguth and V. D. Matterna, *IEEE Phot. Tech. Lett.* **3**, 108 (1991).
- [3] J. A. Lott and R. P. Schneider, Jr., *Electr. Lett.* **29**, 830 (1993).
- [4] B. Tell, R. E. Leibenguth, K. F. Brown-Goebeler and G. Livescu, *IEEE Phot. Tech. Lett.* **4**, 1195 (1992).
- [5] K. H. Gulden, M. Moser, S. Luscher and H. P. Schweizer, *Electr. Lett.* **31**, 2176 (1995).
- [6] J. A. Lott, *Proc. 22nd Int'l Symp. Comp. Semi.* Cheju Island, Korea (Aug 1995).
- [7] K. D. Choquette, R. P. Schneider, Jr., M. Hagerott Crawford, K. M. Geib and J. J. Figiel, *Electr. Lett.* **31**, 1145 (1995).
- [8] W. W. Chow, K. D. Choquette, M. H. Crawford, K. L. Lear and G. R. Hadley, *IEEE J. Quant. Electr.* **33**, 1810 (1997).
- [9] M. H. MacDougall, G. M. Yang, A. E. Bond, C.-K Lin, D. Tishinin and P. D. Dapkus, *IEEE Phot. Tech. Lett.* **8**, 310 (1996).
- [10] R. P. Schneider, Jr., E. D. Jones, J. A. Lott and R. P. Bryan, *J. Appl. Phys.* **72**, 5397–5400 (1992).
- [11] M. J. Noble, J.-H. Shin, K. D. Choquette, J. P. Loehr, J. A. Lott and Y.-H. Lee, *IEEE Photon. Tech. Lett.* **10**, 475 (1998).
- [12] M. J. Noble, J. P. Loehr and J. A. Lott, *IEEE J. Quant. Electr.* **34**, 1890 (1998).